

Research paper

Net-zero stochastic planning for pig farm-dominated rural energy systems considering agricultural demand response

Shuang Kang ^a, Wei Gan ^a, Yue Zhou ^a,* , Ping Ai ^b

^a School of Engineering, Cardiff university, Cardiff, CF24 3AA, Wales, UK

^b College of Engineering, Huazhong Agricultural University, Wuhan, 430070, China



ARTICLE INFO

Keywords:

Rural energy systems
Demand response
Net-zero emissions
Pig farm

ABSTRACT

Given the significant renewable energy potential of rural areas, rural energy systems are emerging as an effective solution to meet local energy demand and achieve net-zero emissions targets. This study proposes a net-zero stochastic planning model for pig farm-dominated rural energy systems, integrating biogas engines, photovoltaic panels, and batteries to economically satisfy local energy demand. First, a comprehensive modelling framework is developed to capture the unique resource availability and energy demand characteristics of pig farms. This includes supplementary lighting requirements for pig growth, biomass availability as well as flexible heating and cooling loads necessary for maintaining optimal farm conditions. Then, a novel operation strategy is introduced, incorporating the flexibility of agricultural demand. It coordinates the demand response mechanism, the battery charging and discharging strategy based on time-of-use electricity prices, and the maximising self-consumption strategy. The demand response mechanism enables price-responsive control of heating and cooling loads by utilising the thermal inertia of pig farms within acceptable temperature limits. Moreover, the net-zero carbon emissions goal for pig farm-dominated rural energy systems is realised using a scenario-based stochastic optimisation method. The approach is demonstrated through a case study of a rural village with a pig farm in Hubei Province, China, illustrating how it can support long-term planning and provide practical guidance for low-carbon rural energy system design. Comparative analyses indicate that the proposed planning model offers both economic and environmental benefits, making it a promising strategy for sustainable rural energy development.

1. Introduction

The goal of improving living standards through economic growth while preserving the planet has inspired policymakers to establish the Sustainable Development Goals (SDGs) for 2030 [1]. This initiative serves as a universal development framework applicable to all countries, with implementation tailored to national priorities. However, traditional energy systems, particularly those heavily reliant on fossil fuels, often face challenges in rural areas, such as high greenhouse gas emissions and elevated costs [2]. The growing urgency to reduce carbon dioxide emissions has positioned renewable energy as a vital alternative to fossil fuels [3]. Rural areas, especially, are rich in renewable resources such as crop residues and animal manure. These materials have significant potential for sustainable energy production through pathways such as biogas generation and direct biomass combustion for electricity generation. Rural energy also plays a crucial role in achieving net-zero goals in many countries, such as the “carbon

peak” and “carbon neutrality” targets in China [4]. In light of this, the study of rural energy systems has gained increasing urgency [5]. Meanwhile, technological advancements are driving the development of rural hybrid energy systems that provide efficient and sustainable solutions for rural areas.

Recent studies on rural energy system optimisation have investigated diverse rural load types, with residential and agricultural loads being the primary focus. For instance, Kumar et al. [6] demonstrated a hybrid off-grid power generation system that integrates solar, biomass, diesel, and battery storage to electrify remote rural communities in eastern India. Zhi et al. [7] proposed a scenario-based optimised sizing and management strategy for a rural photovoltaic (PV)-Battery system to meet farmers’ energy needs. Similarly, Yang et al. [8] established a PV-powered pumped-hydro generator system to reduce reliance on coal-fired electricity, primarily serving household loads in rural China. Moving beyond general rural load considerations, recent

* Corresponding author.

E-mail address: zhouy68@cardiff.ac.uk (Y. Zhou).

<https://doi.org/10.1016/j.enconman.2025.120759>

Received 6 July 2025; Received in revised form 31 October 2025; Accepted 9 November 2025

Available online 10 December 2025

0196-8904/© 2025 The Authors. Published by Elsevier Ltd. This is an open access article under the CC BY license (<http://creativecommons.org/licenses/by/4.0/>).

Nomenclature**Acronyms**

AC	Alternating current
DC	Direct current
GA	Genetic algorithm
GHI	Global horizontal irradiance
GOA	Grasshopper optimisation algorithm
MSC	Maximising self-consumption
PV	Photovoltaic
SDGs	Sustainable Development Goals
SOC	State-of-charge
TOU	Time-of-use
VS	Volatile solid

List of symbols

β	Tilt angle of the surface ($^{\circ}$)
δ	Solar declination angle ($^{\circ}$)
η	Spectral luminous efficacy (lm/W)
η_{bio}	Efficiency of biogas-to-electricity conversion system
η_{ch}, η_{dis}	Battery charging and discharging efficiency
η_{conv}	Conversion efficiency of the converter
γ	Penalty coefficient
κ	Constant indicating gas production rate at a given temperature
λ	Heat transfer coefficient of the wall (kW/(m ² °C))
μ	Proportionality coefficient controlling battery charging amount
ω_1, ω_2	Solar hour angles at the beginning and end of the time period ($^{\circ}$)
ϕ	Latitude ($^{\circ}$)
π^m	Probability of season m (number of days in season/total days in a year)
π_{solar}^m	Probability of solar irradiance scenarios in season m
π_s	Probability of scenario s
ρ^{air}	Indoor air density (kg/m ³)
ρ_g	Ground reflectance
σ	Maximum biogas volume produced per kilogram of volatile solids in a feedstock (m ³ /kg)
A	Heat transfer area of indoor wall (m ²)
a_i, b_i	Initial investment cost and replacement cost for equipment i (CNY per unit capacity)
A_{room}	Room area (m ²)
c^{air}	Specific heat capacity of indoor air (kJ/(kg K))
c_i	Annual maintenance cost per unit capacity for equipment i (CNY per unit capacity)
$C_s^{grid,buy}, C_s^{grid,sell}$	Daily electricity purchase cost and sales revenue from the grid in scenario s (CNY)
$C_{ann,total}$	Total annual cost (CNY)
C_{in}	Annualised investment cost (CNY)
C_{op}	Annual operation cost (CNY)

C_{op}^s	Operation cost under scenario s (CNY)
Cal_{bio}	Calorific value of biogas (kWh/m ³)
Cap^{bat}	Rated battery capacity (kWh)
COP	Coefficient of performance of the heat pump
$CRF(d, l)$	Capital recovery factor
d	Discount rate
$E_s^{grid,imp}, E_s^{grid,exp}$	Daily imported and exported electricity in scenario s (kWh)
$E_t^{bat,in}, E_t^{bat,out}$	Battery charging and discharging energy at time t (kWh)
E_t^{bio}	Electricity from the biogas engine at time t (kWh)
$E_t^{capmax}, E_t^{capmin}$	Maximum and minimum charging/discharging electricity at time t (kWh)
E_t^{exce}	Excess PV generation after satisfying heating/cooling load and battery charging at time t (kWh)
$E_t^{grid,imp}$	Imported electricity from the grid at time t (kWh)
E_t^{hche}	Minimum electricity supplied for heating at time t (kWh)
E_t^{hend}	Maximum electricity supplied for heating at time t (kWh)
E_t^{hc}	Electricity supplied for heating at time t (kWh)
E_t^{load1}	Fixed residential load (kWh)
E_t^{load2}	Pig farm lighting and ventilation loads (kWh)
$E_{s,t}^{grid,imp}, E_{s,t}^{grid,exp}$	Imported and exported electricity at time t in scenario s (kWh)
G_t	Global horizontal irradiance (W/m ²)
G_{sc}	Solar constant (≈ 1367 W/m ²)
I	Global irradiance on a horizontal surface (W/m ²)
I_0	Extraterrestrial irradiance on a horizontal surface (W/m ²)
I_b	Direct beam irradiance (W/m ²)
I_d	Diffuse irradiance (W/m ²)
I_T	Solar irradiation entering the room through windows (W/m ²)
k_T	Clearness index
l	Project lifetime (year)
L_{luxset}	Minimum illuminance required for pig growth (lm/m ²)
$L_{luxsolar}$	Illuminance contribution from solar radiation (lm/m ²)
L_{lux}	Required artificial lighting illuminance (lm/m ²)
M	Number of equipment categories
n	Day of the year
$C_t^{grid,buy}, C_t^{grid,sell}$	Electricity buying and selling prices at time t (CNY/kWh)
$P_{bio,min}, P_{bio,max}$	Minimum and maximum output limits of the biogas engine (kW)
P_{bio}	Rating power of the biogas engine (kW)
P_{carbon}	Penalty function for carbon emissions

$P_{G,i}^{cap}$	Installed capacity of equipment i (kW or kWh)
P_{max}^{bat}	Maximum charging/discharging power of the battery (kW)
P_{max}^{heat}	Maximum power of the heat pump (kW)
PV_{rated}	Rated power of PV panels (kW)
$q_t^{in,min}, q_t^{in,max}$	Minimum and maximum heating/cooling input rates (kW)
q_t^{in}	Heating/cooling input rate (kW)
$q_t^{loss,conduction}$	Thermal energy loss due to conduction (kW)
$q_t^{loss,others}$	Thermal energy loss due to other factors such as air infiltration (kW)
q_t^{loss}	Thermal energy loss per unit time due to conduction, convection, radiation, air infiltration, and cold air penetration (kW)
R	Feedstock retention time (day)
R_b	Tilted surface beam radiation factor (ratio of beam radiation on a tilted surface to that on a horizontal surface)
S_i	Total solids proportion of the fermentation feedstock
S_{bio}	Initial volatile solid concentration in manure and crop residues (kg/m ³)
S_{win}	Window area (m ²)
SOC^{max}, SOC^{min}	Maximum and minimum battery state of charge
SOC_t	Battery state of charge at time t
$T_t^{air,out}$	Outdoor temperature (°C)
T_t^{air}	Indoor temperature (°C)
$Total E_t^{bio}$	Cumulative biogas electricity generation up to time t (kWh)
$Total E_t^{grid,exp}$	Cumulative exported and imported electricity up to time t (kWh)
$Total E_t^{grid,imp}$	Cumulative imported and exported electricity up to time t (kWh)
V^{air}	Indoor air volume (m ³)
V_{bio}	Total daily volume of biogas produced from pig manure and crop straws (m ³)
$V_{d,min}, V_{d,max}$	Minimum and maximum volume limits of the biogas digester (m ³)
W_i	Daily provided fermentation feedstock rate (kg day ⁻¹)
y_i	Replacement year of equipment i (year)
$Y_{p,i}$	Biogas yield of the feedstock (m ³ kg ⁻¹)

studies have refined the modelling of agricultural resources, exemplified by biomass fermentation, alongside agricultural energy demands such as greenhouse thermal loads. These models are further integrated into optimisation frameworks. For example, Fu et al. [9] optimised greenhouse energy management by coordinating crops' lighting, heating loads, and CO₂ consumption with microgrid operations. Li et al. [10] designed a multi-energy system to meet rural energy demands, taking into account irrigation requirements and biomass fermentation. Furthermore, Liu et al. [11] optimised cross-sectoral coordination by coupling power distribution with agricultural supply chains, integrating crop growth, refrigeration, agricultural product transportation, and energy consumption. However, existing studies on rural energy systems have primarily focused on crop-farm loads, such as greenhouses, or on residential loads, while rarely considering energy systems that incorporate livestock farms. In particular, pig farms, which have high energy demands for heating, have received limited attention

despite their crucial role in sustainable rural development. Several studies have specifically examined pig farms. For instance, Kwak et al. [12] and Shin et al. [13] developed energy simulation models for pig farms, focusing on optimising ventilation and heating systems to enhance energy efficiency and sustainability. However, these studies overlooked the mathematical modelling of pig farm loads and failed to incorporate them into planning optimisation frameworks for pig farm-dominated rural energy systems.

For optimal planning of energy systems, an energy management strategy is typically developed. The energy management strategy is commonly defined as an operation strategy that coordinates supply and demand-side management under system constraints to ensure economic, sustainable, and reliable operation [14]. The operation strategy can be classified into two categories: optimisation-based strategies and rule-based strategies [15]. The rule-based strategy applies predefined control rules and logic to manage system operation. Its main advantages over optimisation-based strategies are low computational requirements and independence from future load information [16], making it suitable for real-time applications [17]. Since rule-based operation strategies are logic-driven and consist of if-then rules, priority orders, and threshold-based conditions, they are difficult to represent analytically. This complexity introduces discrete variables, non-convexities, and non-differentiable behaviour into the planning optimisation problem. Although such strategies can, in principle, be reformulated as large-scale mixed-integer programmes, the resulting models are often computationally intractable. Therefore, the problem is typically solved using heuristic algorithms, such as the genetic algorithm (GA), owing to its superior ability to handle complex constraints [18]. The GA has been widely applied in energy system optimisation problems. For example, Ghanbari et al. [19] applied it to a solar-wind-battery desalination system, while Munoz-Pincheira et al. [20] used it to optimise a stand-alone hybrid renewable energy system considering wind-solar complementarity.

The strategy aiming to maximise self-consumption (MSC) of PV generation is one of the most widely used rule-based operation strategies for energy systems [21]. It prioritises renewable energy sources, such as solar power, to supply electricity, with battery storage and the main grid serving as backups to ensure reliability. For instance, Hassan et al. [22] proposed a strategy that uses surplus renewable energy to charge batteries, employs hydropower and biogas to cover deficits, and utilises battery discharge as a backup. Bacha et al. [23] designed a strategy that prioritises renewable energy for battery charging, directs excess energy to a dummy load, discharges the battery when required, and uses diesel as backup. Jaman et al. [24] developed a strategy that charges batteries and produces hydrogen using surplus renewable energy, while employing hydrogen, batteries, and biogas to meet shortfalls. Kallel et al. [25] proposed a control strategy that prioritises solar power, shares surplus energy via a direct current (DC) microgrid, and uses batteries to reduce grid reliance. Another common rule-based strategy that considers the charging and discharging strategy of batteries is the Time-of-use (TOU) strategy. The TOU strategy is adopted to obtain economic benefits by exploiting the difference between peak and off-peak electricity prices. The key principle of the TOU strategy is to charge the battery during off-peak periods using grid electricity and discharge it to the load during peak periods [26]. For example, Liu et al. [27] proposed and validated a photovoltaic (PV) and battery storage system model based on a TOU operation strategy. Liu et al. [28] optimised a PV-battery energy storage system for a low-energy building in China using a novel TOU-based energy management strategy. In rule-based strategies that incorporate demand-side response, electricity price is often an important factor in designing the strategy. For instance, Alimohammadisagvand et al. [29] developed and applied rule-based demand response control strategies for detached-house heating systems under different electricity pricing schemes. Sun et al. [30] developed a building-integrated PV-phase

change material system using a rule-based demand response strategy, where thermostatically controlled loads adjust with time-varying electricity pricing. Considering the substantial heat load demands of rural pig farms, demand-side response to heat loads is of great importance and can contribute to cost reduction. In pig farm-dominated energy systems, both the battery charging and discharging strategies and the demand response considering the flexibility of pig farm loads are crucial; however, studies integrating these two aspects remain scarce. Furthermore, existing studies have rarely integrated these two strategies with the MSC strategy.

While effective operation strategies enhance system performance, achieving truly sustainable rural energy systems requires reducing carbon emissions. Given that agriculture accounts for a large share of greenhouse gas emissions, emission reduction measures in rural areas are essential [31]. Wu [32] developed a low-carbon economic scheduling model that minimises both carbon emissions and operation costs. Jiang et al. [33] proposed a multi-energy complementary, and low-carbon optimised scheduling strategy for eco-agriculture integrated energy systems. However, these studies have not fully achieved the goal of net-zero carbon emissions in rural energy systems. To enable economically viable and stable zero-carbon planning in rural energy systems, various optimisation methods for planning can be considered. Some current research on rural energy systems has focused on deterministic optimisation, which typically uses either year-round datasets or single-month data. Araoye et al. [34] optimised rural hybrid microgrids using HOMER and grasshopper optimisation algorithm (GOA), relying on fixed annual resource and load values. Pal et al. [35] designed an energy system based on the demand in July, which represents the month of peak consumption. However, year-round data-driven planning imposes significant computational burdens, and single-month optimisation often leads to overcapacity or energy deficits in other months. In robust optimisation, only the worst-case results are considered, making the approach overly conservative and economically inefficient [36]. In distributionally robust optimisation, selecting an appropriate ambiguity set and calibrating its parameters are highly challenging [37], and the resulting models are often complex with significant computational burdens. In this study, a risk-neutral, scenario-based stochastic optimisation approach is adopted, as it is straightforward, enhances computational efficiency, and mitigates biased capacity sizing while accounting for long-term seasonal and short-term daily uncertainties in renewable resources such as solar irradiation.

In summary, the research gaps in the existing literature on rural energy systems can be identified as follows: (1) Research on the optimisation of rural energy systems specifically focused on pig farms remains scarce, with limited attention to their load characteristics and energy dynamics. (2) Existing operation strategies have paid limited attention to the demand-side flexibility of pig farms. In particular, the coordination between pigs' biological thermal requirements, time-varying electricity prices, and local renewable energy availability has not been sufficiently explored. (3) Research on the net-zero planning of pig-farm-dominated rural energy systems remains limited.

Considering the limitations of the aforementioned research, this study proposes a net-zero stochastic planning model for pig farm-dominated rural energy systems that incorporates agricultural demand response. The main contributions of this paper are as follows:

(1) A comprehensive framework for pig farm-dominated rural energy systems is proposed, thoroughly considering the unique characteristics of pig farms. The framework includes detailed modelling of both resource availability and load demand, incorporating a biogas production model based on pig manure and crop straws. In addition, supplementary lighting and flexible heating/cooling load models are established, taking into account pigs' growth characteristics and optimal growth environmental requirements.

(2) A novel operation strategy is developed to reduce system costs by integrating agricultural demand flexibility into rural energy management. This strategy coordinates (1) a demand response mechanism that

synchronises pigs' biological thermal requirements with time-of-use electricity prices and (2) a battery charging/discharging strategy based on local renewable availability and time-of-use pricing under the MSC strategy. The demand response mechanism enables price-responsive heating/cooling loads control by adjusting farm's indoor temperature within the permissible range, leveraging the thermal inertia of pig farms.

(3) The net-zero carbon emissions goal for pig farm-dominated rural energy systems planning is achieved using a scenario-based stochastic optimisation method. The approach is applied to a case study of a rural village with a pig farm in Hubei Province, China, demonstrating its capability to support long-term planning, accommodate seasonal and daily fluctuations in renewable energy resources, and provide practical guidance for low-carbon rural energy system design.

The remainder of this paper is organised as follows. Section 2 introduces methodological framework. Section 2.1 outlines the system configuration. The modelling of biomass energy and electrical loads in a pig farm is illustrated in Section 2.2. Section 2.3 details the component models of the energy system. The proposed operation strategy, considering time-of-use prices is presented in Section 2.4. Section 2.5 describes the scenario-based stochastic planning formulation for achieving net-zero carbon emissions. Case study results and discussion are provided in Section 3, where the key findings are analysed and the limitations of the study are discussed. Finally, Section 4 summarises the conclusions and future perspectives.

2. Methods

This section presents the methods used in the study, including the system configuration, the modelling of biomass energy and electrical loads, the modelling of energy system components, the operation strategy, and the net-zero scenario-based stochastic planning model.

2.1. System configuration

The configuration of the pig farm-dominated rural energy system is illustrated in Fig. 1. The rural energy system is connected to the main grid, enabling power transactions based on time-of-use prices. The generating units consist of solar PV panels and biogas modules. Batteries act as a backup, storing excess electricity generated by the PV panels and releasing it when needed. They can also be charged from the main grid by taking advantage of time-of-use prices. Bidirectional converters are installed to facilitate the conversion between alternating current (AC) and DC power. Within the power generation system, electrical demand is primarily met by the PV panels and the biogas module, supported by the batteries and the main grid. The biogas module consists of a digester that converts animal waste and crop residues into biogas, and a biogas engine that utilises this biogas to produce electricity. During the anaerobic fermentation process, animal waste from the pig farm and crop residues are first pumped into the digester. Inside, these organic materials undergo decomposition, producing biogas primarily composed of methane, carbon dioxide, and trace gases. The generated biogas is then used for electricity production, while the resulting slurry is repurposed as effective fertiliser.

As shown in Fig. 1, both residential and agricultural electrical loads are considered in the system. All loads are considered in terms of electricity. The electrical load of rural residents is represented by actual daily profiles. The pig farm loads are considered thoroughly, including lighting, heating and cooling, and ventilation requirements. Moderate temperature, lighting, and ventilation play a crucial role in promoting the pigs' development. Meeting these requirements ensures a suitable living environment for the pigs, which is essential for their growth. The heating and cooling loads are satisfied by electricity-driven heat pumps, a common and feasible solution for modern livestock facilities. Such heat pumps have been shown to reduce energy use and emissions in livestock facilities [38] and to improve environmental performance in agricultural applications [39].

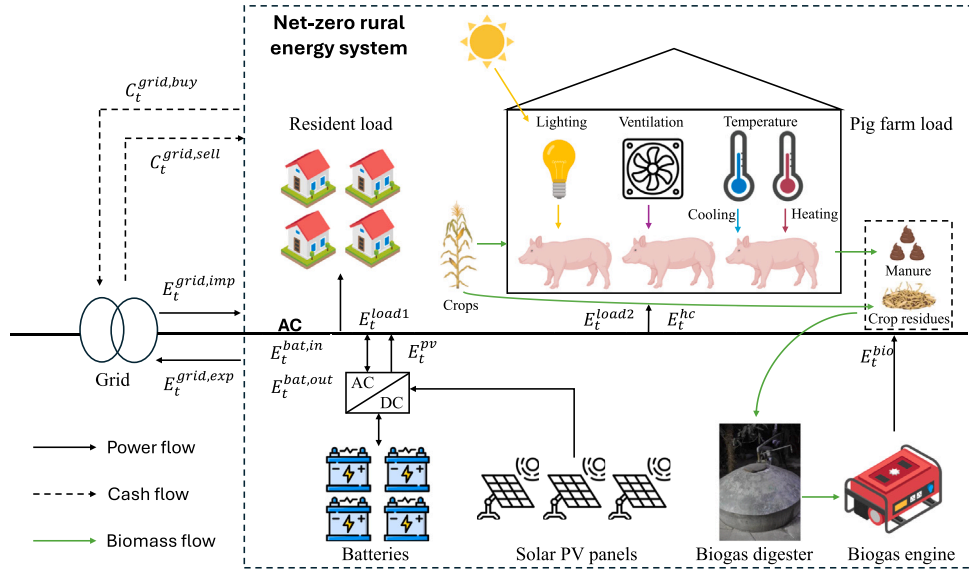


Fig. 1. Configuration of the pig farm-dominated rural energy system.

2.2. Modelling of biomass energy and electrical loads in a pig farm

As the rural energy system is dominated by the pig farm, which accounts for a large proportion of the total load, it is essential to model the farm's resources and loads. Crop residues and pig manure from the farm can be reused to generate electricity. The electrical load modelling of the pig farm considers lighting, heating and cooling, and ventilation demands. The ventilation load is assumed to follow a fixed daily profile, as it represents a relatively small portion of the total energy demand compared with heating and cooling loads [40].

2.2.1. Modelling of biogas potential from livestock waste and crop straws

Crop straws and livestock waste from the pig farm can be utilised for biogas production, which is subsequently used to generate electricity for both the farm and nearby rural households. The biogas potential from pig manure and straws is calculated as follows [41]:

$$V_{bio} = \sum_{i=1}^2 W_i S_i Y_{p,i}, \quad (1)$$

where V_{bio} represents the total daily volume of biogas produced from pig manure and crop straws (m^3); W_i denotes the daily fermentation feedstock rate ($kg \text{ day}^{-1}$); S_i is the total solids proportion of the fermentation feedstock; and $Y_{p,i}$ denotes the biogas yield of the feedstock ($m^3 \text{ kg}^{-1}$).

2.2.2. Modelling of flexible heating and cooling loads

The indoor air in modern pig housing exhibits substantial thermal storage capacity. The thermal inertia effect directly influences the heating and cooling demand of the building [42]. This inherent thermal inertia facilitates the demand-responsive management of heating and cooling loads through a systematic energy dispatch strategy. The optimal indoor temperature for pigs is assumed to be $25 \text{ }^\circ\text{C}$, with an acceptable range between $23 \text{ }^\circ\text{C}$ and $27 \text{ }^\circ\text{C}$. The temperature range is defined based on the varying optimal temperatures for pigs at different stages [43]. The heating and cooling loads are considered flexible, given the pig house's thermal inertia and allowable temperature range.

The dynamic energy balance equation for the building's thermal environment, which describes the energy conservation dynamics of air temperature variations over time in enclosed spaces of pig houses, is given by:

$$q_t^{in} - q_t^{loss} = c^{air} \rho^{air} V^{air} \frac{dT_t^{air}}{dt}, \quad (2)$$

where q_t^{in} represents the heating or cooling input rate, indicating the thermal energy added to or removed from the room per unit time (kW); q_t^{loss} denotes the thermal energy loss per unit time due to conduction, convection, or radiation, air infiltration, and cold air penetration (kW); c^{air} is the specific heat capacity of indoor air ($\text{kJ}/(\text{kg K})$); ρ^{air} is the indoor air density (kg/m^3); V^{air} is the indoor air volume (m^3); and T_t^{air} is the indoor temperature ($^\circ\text{C}$). The primary cause of thermal energy loss is conduction through the walls, driven by the temperature difference between the indoor and outdoor environments. In this study, it is assumed that conduction through the walls contributes significantly, approximately 50%, to the total thermal energy loss in pig housing facilities, based on typical construction and insulation conditions. The total energy loss equation can be expressed as:

$$q_t^{loss} = q_t^{loss,conduction} + q_t^{loss,others}, \quad (3)$$

where $q_t^{loss,conduction}$ denotes the thermal energy loss due to conduction (kW), and $q_t^{loss,others}$ denotes the thermal energy loss attributable to other factors, such as air infiltration (kW). $q_t^{loss,conduction}$ is calculated as follows:

$$q_t^{loss,conduction} = A\lambda(T_t^{air} - T_t^{air,out}), \quad (4)$$

where A represents the heat transfer area of the indoor wall (m^2); $T_t^{air,out}$ denotes the outdoor temperature ($^\circ\text{C}$); and λ indicates the heat transfer coefficient of the wall ($\text{kW}/(m^2 \text{ }^\circ\text{C})$). Parameters in Eqs. (2)–(4) are consolidated using Eq. (5).

$$\begin{cases} A\lambda = \alpha_1 \\ c^{air} \rho^{air} V^{air} = \alpha_2 \end{cases} \quad (5)$$

Substituting Eqs. (4)–(5) into Eq. (2) yields Eq. (6):

$$\begin{cases} \frac{dT_t^{air}}{dt} + \frac{\alpha_1}{\alpha_2} T_t^{air} - \frac{q_t^{in} + \alpha_1 T_t^{air,out}}{\alpha_2} = 0 \\ T_{t,t=0}^{air} = T_{t_0}^{air} \end{cases} \quad (6)$$

By solving the differential equation in Eq. (6) using the midpoint method, the relationship between the heating or cooling input rate (q_t^{in}) and the indoor temperature (T_t^{air}) can be determined, resulting in explicit expressions for q_t^{in} and T_t^{air} , as presented in Eqs. (7) and (8).

$$q_t^{in} = \left(\frac{\alpha_1}{2} + \frac{\alpha_2}{3600}\right) T_t^{air} + \left(\frac{\alpha_1}{2} - \frac{\alpha_2}{3600}\right) T_{t-1}^{air} - \alpha_1 T_{t-1}^{air,out} \quad (7)$$

$$T_t^{air} = \frac{(q_t^{in} + \alpha_1 T_t^{air,out} - T_{t-1}^{air} (\frac{\alpha_1}{2} - \frac{\alpha_2}{3600}))}{(\frac{\alpha_1}{2} + \frac{\alpha_2}{3600})} \quad (8)$$

The minimum and maximum heating or cooling inputs are calculated by substituting the temperature bounds (T^{airmin} and T^{airmax}) into Eq. (7), yielding:

$$q_t^{in,min} = (\frac{\alpha_1}{2} + \frac{\alpha_2}{3600})T^{airmin} + (\frac{\alpha_1}{2} - \frac{\alpha_2}{3600})T_{t-1}^{air} - \alpha_1 T_t^{air,out}, \quad (9)$$

$$q_t^{in,max} = (\frac{\alpha_1}{2} + \frac{\alpha_2}{3600})T^{airmax} + (\frac{\alpha_1}{2} - \frac{\alpha_2}{3600})T_{t-1}^{air} - \alpha_1 T_t^{air,out}, \quad (10)$$

where T^{airmin} and T^{airmax} denote the minimum and maximum allowable indoor temperatures for heating and cooling, respectively ($^{\circ}\text{C}$).

2.2.3. Modelling of supplementary lighting loads

Previous studies have shown that appropriate lighting is essential for the growth and welfare of pigs [44]. In this study, artificial lighting is used as a supplement to meet the required illumination when solar radiation is insufficient.

The required artificial lighting, excluding the contribution from solar irradiation, is calculated as:

$$L_{lux} = L_{luxset} - L_{luxsolar}, \quad (11)$$

where L_{lux} is the required artificial lighting illuminance (lm/m^2); L_{luxset} is the minimum illuminance required for pig growth (lm/m^2); and $L_{luxsolar}$ is the illuminance contributed by solar radiation entering through windows (lm/m^2). The illuminance contribution from solar radiation, $L_{luxsolar}$, is calculated as:

$$L_{luxsolar} = \frac{I_T S_{win} \eta}{A_{room}}, \quad (12)$$

where I_T is the solar irradiance entering the room through the windows (W/m^2); S_{win} is the window area (m^2); η is the spectral luminous efficacy (lm/W); and A_{room} is the room area (m^2). The total solar irradiance I_T on the inclined window surfaces can be calculated as follows, assuming that the pig house has windows facing two opposite directions [45]:

$$I_T = I_b R_b + 2I_d \left(\frac{1 + \cos \beta}{2} \right) + 2I_g \rho_g \left(\frac{1 - \cos \beta}{2} \right), \quad (13)$$

where I_b is the direct beam irradiance (W/m^2); R_b is the tilted surface beam radiation factor, defined as the ratio of beam radiation on a tilted surface to that on a horizontal surface; I_d is the diffuse irradiance (W/m^2); I is the global irradiance on a horizontal surface (W/m^2); ρ_g is the ground reflectance (albedo); and β is the tilt angle of the surface (set to 90° in this analysis). The tilted surface beam radiation factor R_b is given by:

$$R_b = \frac{\cos(\phi - \beta) \cos \delta \cos \frac{\omega_1 + \omega_2}{2} + \sin(\phi - \beta) \sin \delta}{\cos \phi \cos \delta \cos \frac{\omega_1 + \omega_2}{2} + \sin \phi \sin \delta}, \quad (14)$$

where ϕ is the latitude ($^{\circ}$); δ is the solar declination angle ($^{\circ}$); and ω_1 , ω_2 denote the solar hour angles at the beginning and end of the time period ($^{\circ}$). Given the global irradiance I , the direct and diffuse components, I_b and I_d , can be obtained using Eqs. (15)–(18),

$$I_b + I_d = I, \quad (15)$$

$$\frac{I_d}{I} = \begin{cases} 1.0 - 0.249k_T, & \text{for } 0 \leq k_T \leq 0.35 \\ 1.557 - 1.84k_T, & \text{for } 0.35 < k_T < 0.75, \\ 0.177, & \text{for } k_T > 0.75 \end{cases} \quad (16)$$

where $\frac{I_d}{I}$ is the fraction of diffuse irradiance, and k_T is the clearness index, which represents the atmospheric condition. The clearness index k_T is subject to Eqs. (17) and (18). The clearness index k_T is calculated as follows:

$$k_T = \frac{I}{I_o}, \quad (17)$$

where I_o is the extraterrestrial irradiance on a horizontal surface (W/m^2). I_o is calculated as follows [45]:

$$I_o = \frac{12 \times 3600}{\pi} G_{sc} \left(1 + 0.033 \cos \frac{360n}{365} \right) \left[\cos \phi \cos \delta (\sin \omega_2 - \sin \omega_1) + \frac{\pi(\omega_2 - \omega_1)}{180} \sin \phi \sin \delta \right], \quad (18)$$

where G_{sc} is the solar constant (approximately $1367 \text{ W}/\text{m}^2$), and n denotes the day of the year.

2.3. Modelling of energy system components

The proposed rural energy system mainly consists of PV panels, a biogas digester, biogas engines, and batteries.

2.3.1. PV modelling

Solar panels convert solar energy into electrical energy. The output power of the PV module is calculated as [35]:

$$P_t^{pv} = \frac{G_t}{1000} PV_{rated}, \quad (19)$$

where G_t denotes the global horizontal irradiance (GHI) (W/m^2), and PV_{rated} represents the rated power of PV panels (kW).

The electricity generated by the PV module during time period t is given by [35]:

$$E_t^{pv} = P_t^{pv} \Delta t \eta_{conv}, \quad (20)$$

where Δt denotes the operation duration (1 h), and η_{conv} represents the conversion efficiency of the converter.

2.3.2. Biogas modelling

The biogas produced in the digester drives a biogas engine for electricity generation. The total electricity generated from biogas in a day is calculated as [35]:

$$E_{bio}^{total} = V_{bio} Cal_{bio} \eta_{bio}, \quad (21)$$

where V_{bio} is the total volume of biogas available for supply to the biogas engine (m^3), as shown in Eq. (1); Cal_{bio} is the calorific value of biogas (kWh/m^3); and η_{bio} is the system efficiency of biogas-to-electricity conversion.

The required volume of the digester is determined by [35]:

$$V_d = \frac{V_{bio}}{\sigma \left(\frac{\kappa}{1 + \kappa R} \right) S_{bio}}, \quad (22)$$

where σ is the maximum amount of biogas that can be produced from 1 kg of volatile solids in a feedstock (m^3/kg); κ is a constant indicating the rate of gas production at a given temperature; R is the feedstock retention time (day); and S_{bio} is the initial volatile solid (VS) concentration in the animal manure and crop residues (kg/m^3).

2.3.3. Battery modelling

Batteries serve as a reliable backup power source when other generation components fail to meet the load demand. They also perform an arbitrage function by charging during periods of low electricity prices and discharging during high-price periods. Batteries therefore play a vital role in ensuring reliable electricity supply in the rural energy system. The state-of-charge (SOC) is the ratio of the energy stored in the battery to its total rated capacity (Cap^{bat}) and is calculated as [46]:

$$SOC_t = SOC_{t-1} + \frac{E_t^{bat,in} \eta_{ch}}{Cap^{bat}} + \frac{E_t^{bat,out}}{Cap^{bat} \eta_{dis}}, \quad (23)$$

where SOC_t denotes the charge state of the battery at time t ; $E_t^{bat,in}$ and $E_t^{bat,out}$ represent the charging and discharging energy of the battery at t th hour ($E_t^{bat,out} < 0$) (kWh); and η_{ch} and η_{dis} are the charging and discharging efficiency of the battery, respectively.

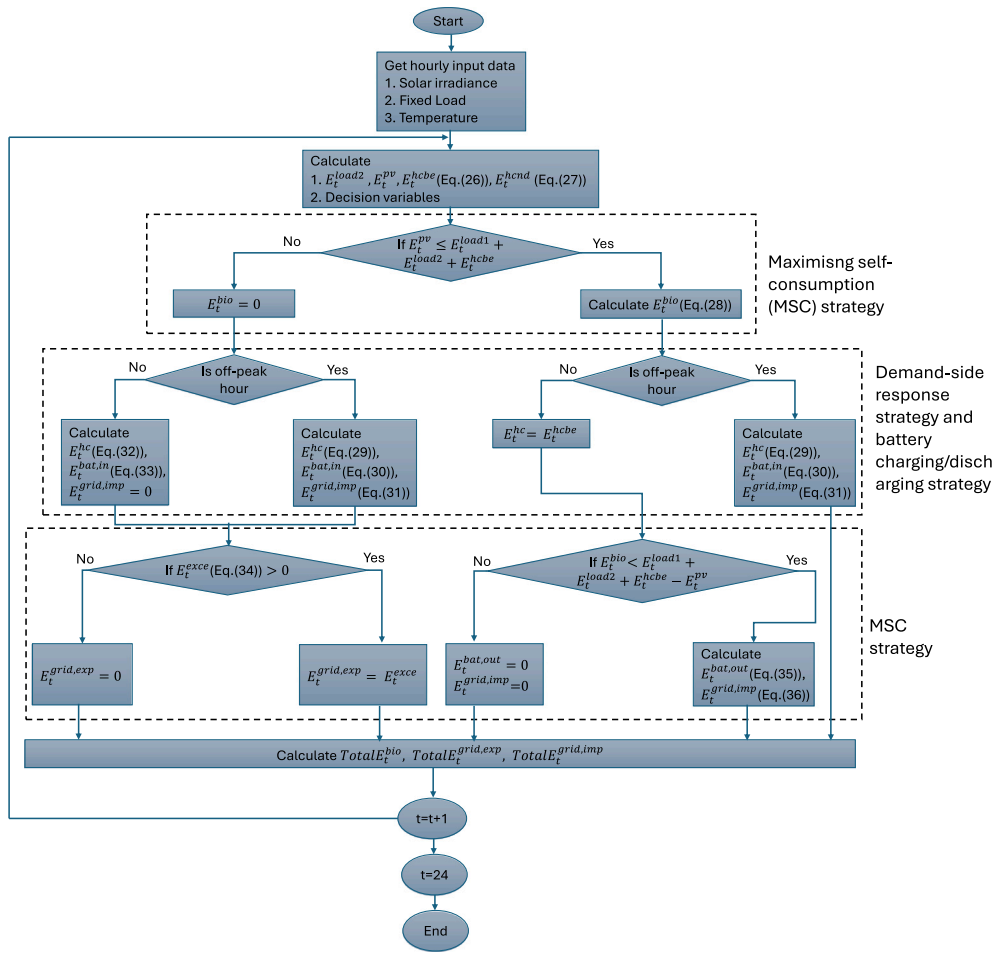


Fig. 2. Operation strategy flowchart of the rural energy system.

The maximum and minimum charging and discharging electricity at t th hour, denoted as E_t^{capmax} and E_t^{capmin} are determined by:

$$E_t^{capmax} = \frac{(SOC^{max} - SOC_{t-1})Cap^{bat}}{\eta_{ch}}, \quad (24)$$

$$E_t^{capmin} = (SOC_{t-1} - SOC^{min})Cap^{bat}\eta_{dis}, \quad (25)$$

where E_t^{capmax} is the maximum electricity that can be charged to reach the maximum state of charge at time t (kWh); E_t^{capmin} is the maximum electricity that can be discharged to reach the lower SOC limit (kWh); and SOC^{max} and SOC^{min} are the maximum and minimum SOC, respectively.

2.4. Operation strategy considering demand-side response and time-varying electricity prices

The operation strategy coordinates PV generation, biogas, battery storage, and the main grid to optimise energy distribution and maximise renewable energy utilisation. The following subsections present the maximum self-consumption strategy, the demand-side response strategy, and the battery charging/discharging strategy, with consideration of time-varying electricity prices.

2.4.1. Operation strategy description

The operation strategy integrates the MSC strategy, the demand-side response, and the battery charging/discharging strategies, taking electricity pricing into account. In the MSC strategy, the rural energy system prioritises PV generation to satisfy electricity demand. During solar power deficits, the biogas engine compensates for the shortfall,

while the batteries and the main grid provide supplementary supply. The storage system can be charged using either surplus PV generation or grid electricity during low-price periods, and any remaining excess PV electricity is exported to the grid.

Considering time-of-use electricity pricing with peak, mid-peak, and off-peak periods, the demand-side response and battery charging/discharging strategies are incorporated into the operation strategy to shift peak loads and minimise system costs. The rural energy system operates under the following strategies aside from the MSC strategy:

(1) The demand-side response strategy accounts for TOU electricity pricing by dynamically adjusting the heating/cooling loads in the pig farm in response to varying electricity rates. During peak and mid-peak periods, the strategy prioritises meeting basic heating/cooling need, maintaining the indoor temperature at the lower bound. Surplus PV generation, if available, is used to increase indoor temperature. If PV generation is insufficient to meet the basic heating/cooling demand, biogas engine supplements the load, with battery storage and grid power serving as backups. During off-peak periods, PV and grid power are used to meet the maximum heating/cooling load, raising the indoor temperature to the upper bound and effectively transforming the pig house into a thermal energy storage system.

(2) The charging and discharging strategy of the batteries also considers time-of-use electricity pricing, adjusting battery operation based on varying electricity rates. During peak and mid-peak periods, surplus PV energy is first used to charge the batteries. When PV and biogas generation cannot meet the load, the batteries are discharged to bridge the gap. During off-peak periods, batteries are fully charged using excess PV energy, if available, along with electricity from the grid.

2.4.2. Overall operation strategy

The overall operation strategy is illustrated in Fig. 2. The strategy consists of the MSC strategy, the demand-side response strategy, and the battery charging and discharging strategy. At each time step, the heating and cooling inputs are adjusted according to the time-varying electricity price, under the constraint that the indoor temperature remains within the permissible range. The strategy also determines, at each time step, the output of the generation units, the charging and discharging behaviour of the battery, and the electricity exchange with the grid to meet demand.

Taking the heating demand scenario as an example, hourly irradiance data, fixed residential electricity consumption, and outdoor temperature are used as inputs. The decision variables are then generated. All variables prefixed with E in the following equations are expressed in kilowatt-hours (kWh). First, the minimum and maximum heating supply E_t^{hcbe} and E_t^{hcnd} are calculated as:

$$E_t^{hcbe} = \frac{q_t^{in,min}}{COP} \Delta t, \quad (26)$$

$$E_t^{hcnd} = \frac{q_t^{in,max}}{COP} \Delta t, \quad (27)$$

where E_t^{hcbe} is the minimum supplied electricity for heating at time t ; COP is the coefficient of performance of the heat pump; and E_t^{hcnd} is the maximum supplied electricity for heating at time t .

In the MSC strategy, if PV generation exceeds the basic load, the biogas engine output is set to zero. If PV generation cannot meet the basic load, the biogas engine is activated. The biogas engine generation E_t^{bio} is given by:

$$E_t^{bio} = \min \left\{ E_t^{load1} + E_t^{load2} + E_t^{hcbe} - E_t^{pv}, P_{bio} \Delta t, E_{bio}^{total} - Total E_t^{bio} \right\}, \quad (28)$$

where P_{bio} is the rating power of the biogas engine (kW), and $Total E_t^{bio}$ is the cumulative biogas electricity generation up to time t .

In the demand-side response and battery charging/discharging strategies, if PV generation exceeds the basic load and hour t is an off-peak period, the heating supply (E_t^{hc}), the battery charging energy ($E_t^{bat,in}$), and the imported electricity ($E_t^{grid,imp}$) are calculated as follows:

$$E_t^{hc} = \min(E_t^{hcnd}, P_{max}^{heat} \Delta t), \quad (29)$$

$$E_t^{bat,in} = \min(P_{max}^{bat} \Delta t, \mu E_t^{capmax}), \quad (30)$$

$$E_t^{grid,imp} = \max(E_t^{load1} + E_t^{load2} + E_t^{hc} - E_t^{pv} - E_t^{bio} + E_t^{bat,in}, 0), \quad (31)$$

where E_t^{hc} is the electricity supplied for heating at time t ; P_{max}^{heat} is the maximum power of the heat pump (kW); P_{max}^{bat} is the maximum charging and discharging power of the battery (kW); μ is a proportionality coefficient used to control the battery charging amount; $E_t^{grid,imp}$ is the imported electricity from the grid at time t ; E_t^{bio} is the electricity provided by the biogas engine at time t ; E_t^{load1} is the fixed residential load; and E_t^{load2} represents the lighting and ventilation loads of the pig farm.

Otherwise, $E_t^{grid,imp} = 0$, and E_t^{hc} and $E_t^{bat,in}$ are calculated as:

$$E_t^{hc} = \min \left\{ E_t^{hcnd}, P_{max}^{heat} \Delta t, E_t^{pv} - E_t^{load1} - E_t^{load2} + E_t^{bio} \right\}, \quad (32)$$

$$E_t^{bat,in} = \min \left\{ P_{max}^{bat} \Delta t, \mu E_t^{capmax}, E_t^{pv} + E_t^{bio} - E_t^{load1} - E_t^{load2} - E_t^{hc} \right\}. \quad (33)$$

If PV generation is insufficient and hour t is an off-peak period, E_t^{hc} , $E_t^{bat,in}$, and $E_t^{grid,imp}$ are determined using Eqs. (29)–(31); otherwise, only the basic load demand is satisfied.

In the MSC strategy, if PV generation exceeds the basic load, the excess electricity (E_t^{exce}) is calculated as:

$$E_t^{exce} = E_t^{pv} - E_t^{load1} - E_t^{load2} - E_t^{hc} - E_t^{bat,in}, \quad (34)$$

where E_t^{exce} represents the surplus PV generation after meeting the heating load and charging the batteries at time t . Any excess electricity, if available, is exported to the grid. If PV generation is not enough, and it is not an off-peak period, and the biogas output can meet the basic load, then $E_t^{bat,out} = 0$ and $E_t^{grid,imp} = 0$; otherwise, if the biogas output cannot meet the basic load, they are calculated as:

$$E_t^{bat,out} = -\min \left\{ E_t^{load1} + E_t^{load2} + E_t^{hc} - E_t^{pv} - E_t^{bio}, P_{max}^{bat} \Delta t, E_t^{capmin} \right\}, \quad (35)$$

$$E_t^{grid,imp} = E_t^{load1} + E_t^{load2} + E_t^{hc} - E_t^{pv} - E_t^{bio} + E_t^{bat,out}. \quad (36)$$

Finally, the cumulative totals $Total E_t^{bio}$, $Total E_t^{grid,exp}$, and $Total E_t^{grid,imp}$ are updated, representing the total biogas generation, exported electricity, and imported electricity up to time t , respectively. During the final hours of the day, the batteries will be charged or discharged to ensure that the end-of-day SOC matches the initial SOC.

2.5. Net-zero scenario-based stochastic planning

A scenario-based stochastic planning model is employed to tackle the uncertainties associated with solar irradiance. The model determines the optimal system configuration with the objective of minimising the system costs while achieving the net-zero emissions target.

2.5.1. Scenario generation

As illustrated in Fig. 3, seasonal variations are incorporated into the model. The seasonal characteristics of power generation and electric load data are considered, and representative days for spring, summer, autumn, and winter are extracted using the K-means clustering method. Seasonal data are represented by the months of March, June, September, and December. The specific procedure is elaborated as follows [46].

(1) The historical monthly data of solar irradiance and electric load are divided into four datasets corresponding to the four seasons. The electric load profiles are represented by four typical seasonal scenarios.

(2) K-means clustering is applied to each seasonal solar irradiance dataset. Taking spring as an example, the dataset is clustered into three groups, yielding three representative scenarios and their corresponding probabilities.

In total, 12 representative scenarios are obtained to capture both seasonal and annual variations in solar resources and electrical loads. The operation strategy is implemented on a 24-hour basis with hourly resolution within each scenario, reflecting the typical daily operation pattern of the pig farm energy system. In contrast, the stochastic planning is performed on an annual basis to capture long-term system behaviour. This approach enables the operation strategies to be applied within each scenario while ensuring that the planning reflects annual system variability, thus providing a tractable yet realistic modelling framework.

The probability π_s of each scenario s is calculated as [47]:

$$\pi_s = \pi^m \pi_{solar}^m, \quad (37)$$

where π^m is the probability of the seasons and is equal to the ratio of the days of the season to the total days of the year, and π_{solar}^m is the probability of solar irradiance scenarios in season m , calculated as the ratio of scenario days to the total days in the month.

2.5.2. Net-zero driven optimisation

The net-zero driven optimisation framework is further elaborated in the following subsections, including the objective function and the associated constraints.

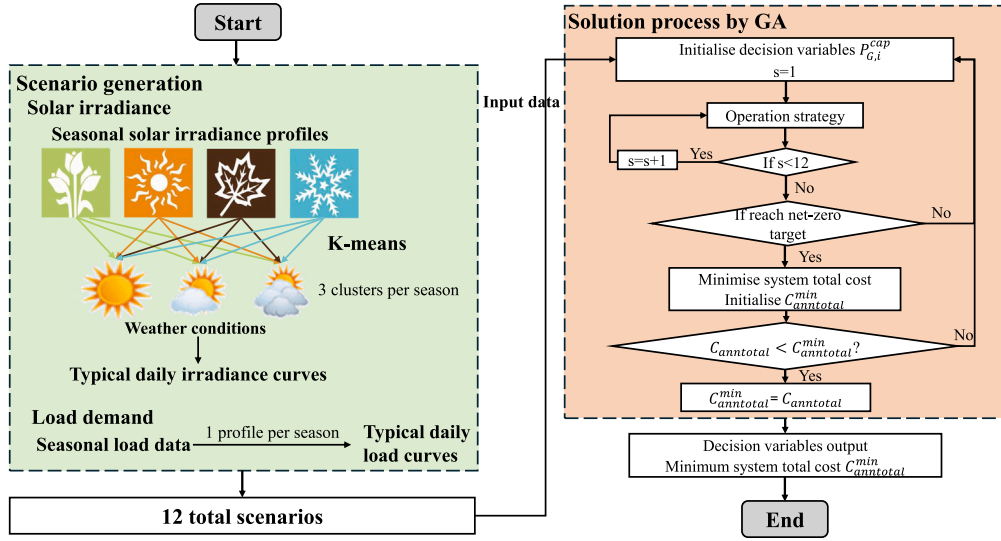


Fig. 3. Framework flowchart of the scenario-based stochastic planning model.

2.5.2.1. Objective function. The risk-neutral stochastic optimisation method is applied. The objective of the optimisation model is to minimise total annual costs under the carbon neutrality constraint. To rigorously enforce zero carbon emissions, a penalty function quantifying carbon output is incorporated into the optimisation formulation. The optimal planning problem is solved using a GA. The objective function is expressed as:

$$\min F = C_{ann,total} + P_{carbon}, \quad (38)$$

where $C_{ann,total}$ denotes the total annual cost (CNY), and P_{carbon} represents the carbon-penalty function.

The total annual cost comprises the annualised investment cost and annual operation cost. The total annual cost is calculated as:

$$C_{ann,total} = C_{in} + C_{op}, \quad (39)$$

$$C_{op} = 365 \sum_{s=1}^S \pi_s C_{op}^s, \quad (40)$$

where C_{op}^s is the operation cost of scenario s (CNY).

The investment cost includes the total acquisition cost over the project lifetime covering both initial investment cost and replacement cost. The annualised equipment investment cost is obtained by amortising the total lifecycle expenditure using a capital recovery factor. It is given by [48]:

$$C_{in} = CRF(d, l) \sum_{i=1}^M \left[(a_i + b_i / (1 + d)^{y_i}) P_{G,i}^{cap} \right], \quad (41)$$

where l represents the lifetime of the project (year); d denotes the discount rate; M represents the number of equipment categories; a_i and b_i are the equipment initial investment cost and replacement cost (CNY per unit capacity); y_i denotes the replacement year of equipment i (year); and $P_{G,i}^{cap}$ is the capacity for equipment i (kW or kWh). The capital recovery factor, which converts the total investment into an equivalent annualised cost, is defined as:

$$CRF(d, l) = \frac{d(1 + d)^l}{(1 + d)^l - 1}. \quad (42)$$

The system operation cost comprises the cost of purchased electricity, the revenue from electricity sales, and equipment maintenance expenses. The annual operation cost C_{op} is calculated using Eqs. (43)–(45):

$$C_{op} = 365 \sum_{s=1}^S \pi_s (C_s^{grid,buy} - C_s^{grid,sell}) + \sum_{i=1}^M c_i P_{G,i}^{cap}, \quad (43)$$

$$C_s^{grid,buy} = \sum_{t=1}^{24} E_{s,t}^{grid,imp} C_t^{grid,buy}, \quad (44)$$

$$C_s^{grid,sell} = \sum_{t=1}^{24} E_{s,t}^{grid,exp} C_t^{grid,sell}, \quad (45)$$

where $C_s^{grid,buy}$ and $C_s^{grid,sell}$ are the daily electricity purchase cost and sales revenue from the grid in scenario s , respectively (CNY); c_i is the annual maintenance cost of unit capacity of equipment i (CNY per unit capacity); $E_{s,t}^{grid,imp}$ and $E_{s,t}^{grid,exp}$ are the imported and exported electricity at time t in scenario s , respectively (kWh); and $C_t^{grid,buy}$ and $C_t^{grid,sell}$ are the prices of buying and selling electricity at time t (CNY).

The carbon penalty function quantifies annual carbon emissions based on the net grid electricity imports. Renewable generation and biomass are assumed to be carbon-neutral, and all system emissions are attributed to grid electricity purchases. The penalty function P_{carbon} is given by Eqs. (46)–(48):

$$P_{carbon} = \gamma \left| 365 \sum_{s=1}^S \pi_s (E_s^{grid,imp} - E_s^{grid,exp}) \right|, \quad (46)$$

$$E_s^{grid,exp} = \sum_{t=1}^{24} E_{s,t}^{grid,exp}, \quad (47)$$

$$E_s^{grid,imp} = \sum_{t=1}^{24} E_{s,t}^{grid,imp}, \quad (48)$$

where γ is the penalty coefficient, and $E_s^{grid,imp}$ and $E_s^{grid,exp}$ are the total daily imported and exported electricity in scenario s (kWh).

2.5.2.2. Constraints. The objective function is subject to the following constraints:

(1) Equipment capacity constraints. The equipment capacity is restricted by:

$$P_{G,i}^{cap,min} \leq P_{G,i}^{cap} \leq P_{G,i}^{cap,max}. \quad (49)$$

(2) Energy balance constraint. At each time step t , the total input and output energy must remain balanced, as expressed in Eq. (50):

$$\begin{cases} E_t^{pv} + E_t^{bio} + E_t^{grid,imp} = E_t^{load} + |E_t^{hc}| + \\ E_t^{bat,in} + E_t^{bat,out} + E_t^{grid,exp} \end{cases} \quad (50)$$

Eqs. (31) (34) (36)

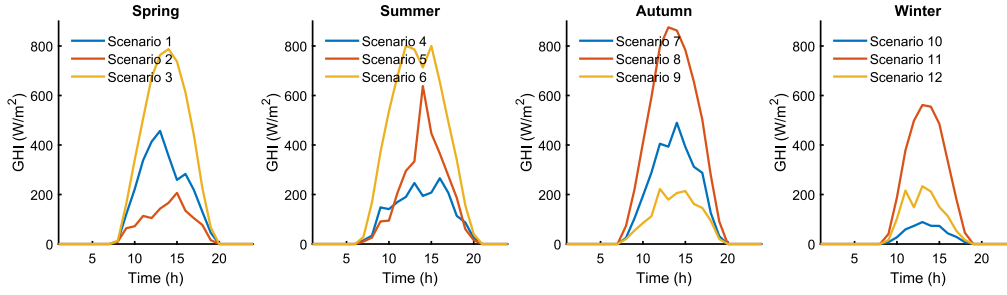


Fig. 4. Extracted 3 typical daily solar irradiance scenarios of each season by k-means clustering.

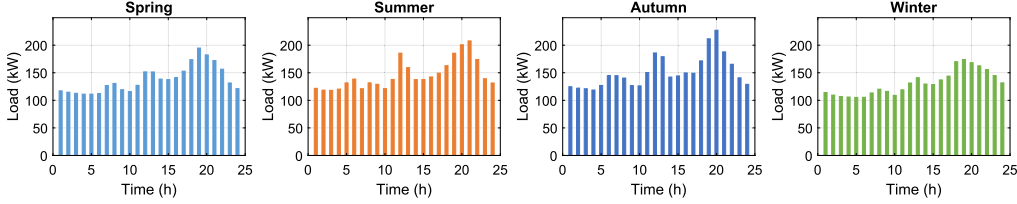


Fig. 5. The typical profiles of fixed load under different seasons.

(3) Constraints for power generation and biogas digester. Eq. (51) defines the upper and lower output limits for power generators and the biogas digester:

$$\begin{cases} P_{bio,min}\Delta t \leq E_t^{bio} \leq P_{bio,max}\Delta t \\ 0 \leq P_t^{pv} \leq P_t^{pv, rated} \\ V_{d,min} \leq V_d \leq V_{d,max} \\ \text{Eqs. (19) (20) (21) (22) (28)} \end{cases} \quad (51)$$

where $P_{bio,min}$, $P_{bio,max}$ are the minimum and maximum output limits of the biogas engine (kW), respectively, and $V_{d,min}$ and $V_{d,max}$ represent the minimum and maximum volume limits of the biogas digester (m^3).

(4) Constraints for the battery energy storage system. The constraints of the storage battery are formulated as follows:

$$\begin{cases} SOC_{1,0} = SOC^{min} \\ SOC^{min} \leq SOC_t \leq SOC^{max} \\ SOC_{s,0} = SOC_{s,24} = SOC_{s+1,0} \\ P_t^{bat,in} \leq P_{bat}^{max} \\ |P_t^{bat,out}| \leq P_{bat}^{max} \\ \text{Eqs. (23) (24) (25) (30) (33) (35)} \end{cases} \quad (52)$$

(4) Constraints for the heating and cooling load. The heating and cooling load constraints are expressed as follows:

$$\begin{cases} T_{s,0}^{air} = T_{s,24}^{air} \\ \text{Eqs. (26) (27) (29) (32)} \end{cases} \quad (53)$$

3. Results and discussion

This section presents the case study setup, the results of the case study, including the optimal outcomes of the proposed rural energy system planning model, comparative analyses with other models, and a discussion of the findings and the limitations of the study.

3.1. Case study setup

The case study is conducted on a rural energy system located in Hubei Province, China, where the prototype village includes a pig farm. This analysis demonstrates the effectiveness of the proposed model. Typical daily solar irradiance scenarios are extracted from annual global horizontal irradiance data, obtained from the National Solar Radiation Database (NSRDB) [49], as illustrated in Fig. 4. The

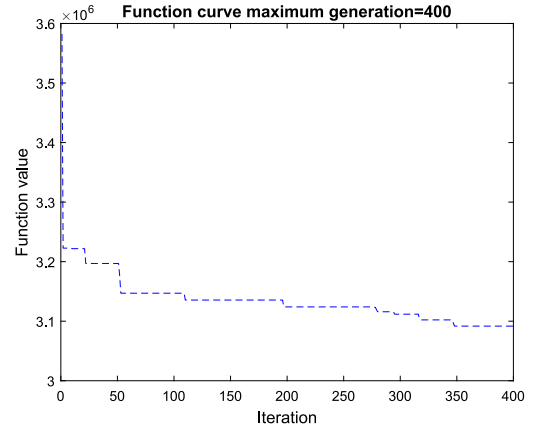


Fig. 6. Convergence curve of the GA.

K-means clustering is performed using squared Euclidean distance as the similarity measure, k-means++ initialisation, a maximum of 100 iterations, and a single replicate. Here, k-means++ initialisation is an improved method for selecting initial cluster centres, which enhances convergence speed and clustering stability, while a single replicate indicates that the algorithm is executed only once, rather than multiple times to select the best solution. The fixed residential load data are derived from historical records and data from comparable villages [50]. Similarly, fixed ventilation load data are estimated based on historical data and operational parameters from similar pig farms [12]. Fig. 5 shows the typical daily profiles of the sum of the two fixed loads. The key technical parameters of the system components are listed in Table 1. The project lifetime is set to 20 years. The technical specifications of the battery and biogas system are shown in Tables 2 and 3, respectively. Table 4 gives the time-of-use electricity prices adopted in the simulation.

All simulations are implemented on a personal computer equipped with a CPU: 11th Gen Intel(R) Core(TM) i7-1165G7 @ 2.80 GHz 1.69 GHz and 16.0 GB of RAM.

3.2. Optimal results of the proposed rural energy system planning model

The proposed rural energy system planning is solved using a GA. The convergence behaviour of the GA is shown in Fig. 6. The optimal

Table 1
Components parameters.

Component	Rated capacity	Capital cost/CNY	Replacement cost/CNY	Maintenance cost/CNY/yr	Lifetime/yr
Solar PV	1 kW	5100	5100	150	20
Biogas engine	3 kW	10,000	10,000	300	5
Biogas digester	1 m ³	300	300	10	20
Li-on battery	10 kWh	10,000	10,000	800	10
Bidirectional converter	1 kW	1000	1000	50	20

Table 2
Specification of the battery.

Indicator	Unit	Value
Rated capacity	kWh	10
Charge and discharge efficiency	%	93
Maximum charge power	kW	2
SOC^{min}	%	10
SOC^{max}	%	90

Table 3
Specification of the biogas system.

Indicator	Unit	Value
Biogas engine rated capacity	kWh	3
Calorific value of biogas	kWh/m ³	5.46
Overall efficiency of biogas system	%	25

Table 4
Time-of-use electricity prices.

Time	Purchase price (CNY/kWh)	Sales price (CNY/kWh)
Peak hours 7:00–12:00, 18:00–22:00	1.062	0.85
Mid-peak hours 12:00–18:00, 22:00–00:00	0.637	0.57
Off-peak hours 00:00–7:00	0.312	0.22

configuration results of the proposed rural model are summarised in Table 5. The optimal total annual cost is 3,091,340 CNY, as shown in Table 7.

Under the net-zero emissions constraint, the optimal installed capacity of solar PV panels is 4626 kW. This is because, after meeting the load demand, the PV system must generate additional electricity for export to the grid to ensure net-zero emissions. The installed capacity of the bidirectional converter is 3888 kW, required to convert the PV output from DC to AC power. The biogas engine capacity is 276 kW, limited by the daily biogas production volume. The capacity of batteries is 350 kWh, serving as an auxiliary energy buffer in the system.

Fig. 7 displays the operation results of the proposed model in different scenarios. From 00:00 to 07:00, the load is supplied by the biogas engine and electricity purchased from the grid due to the absence of solar radiation, while the batteries are charged by the grid because it is off-peak hours. From 07:00 to 18:00, the PV output meets the load due to the sufficient solar radiation, and any excess electricity is exported to the grid. From 18:00 to 00:00, the biogas engine is activated to compensate for the lack of solar irradiance, while the battery is discharged and additional electricity is purchased from the grid to meet the demand. In summer, the PV system exports a larger amount of electricity to the grid because of the higher solar irradiance compared to other seasons. In winter, lower solar irradiance results in greater reliance on grid electricity to meet the load demand.

Fig. 8 shows the flexible heating and cooling load results in different scenarios. In summer, cooling is required, while heating is needed in other seasons. During the initial hours, the heating/cooling load is relatively high because these periods correspond to off-peak hours. the system purchases electricity from the grid to satisfy the heating or cooling demand required to maintain the indoor temperature at

Table 5
Optimal component sizes with carbon constraint.

Component	Parameter	Value
Solar PV	PV_{rated}	4626 kW
Biogas engine	P_{bio}	276 kW
Battery energy storage system	Cap^{bat}	350 kWh
Bidirectional AC–DC converter	P_{conv}	3888 kW

Table 6
Optimal component sizes without carbon constraint.

Component	Parameter	Value
Solar PV	PV_{rated}	120 kW
Biogas engine	P_{bio}	234 kW
Battery energy storage system	Cap^{bat}	170 kWh
Bidirectional AC–DC converter	P_{conv}	101 kW

Table 7
Cost and carbon emissions for systems with/without carbon constraint.

Value	Case 1 with carbon constraint	Case 2 without carbon constraint
Total annual cost/CNY	3,091,340	2,647,370
Annualised equipment expenditure/CNY	3,733,189	459,613
Annual net electricity purchase cost/CNY	−641,849	2,187,757
Annual net electricity import/kWh	−43.6	4,156,504
Annual net carbon emissions/kg	−21.8	2,078,252

Table 8
Cost for systems with different control strategies.

Cost/CNY	Case 1 with the novel operation strategy	Case 3 with the MSC operation strategy
Total annual cost	3,091,340	3,521,711
Annualised equipment expenditure	3,733,189	3,529,475
Annual electricity purchase cost	1,493,227	2,064,501
Annual electricity sales revenue	2,135,076	2,072,265

its upper or lower bound. Heating loads in spring and autumn are relatively high because of lower outdoor temperatures, which require additional heat input to maintain the desired indoor temperature. The indoor temperature curves remain within the specified permissible range throughout all scenarios.

3.3. Comparison results

To verify the effectiveness of the proposed rural energy system planning model, the following three cases are compared:

Case 1: The proposed system planning model incorporating a net-zero emissions constraint and a novel operation strategy considering agricultural demand response.

Case 2: The system planning model that adopts the same operation strategy but excludes the net-zero emissions constraint.

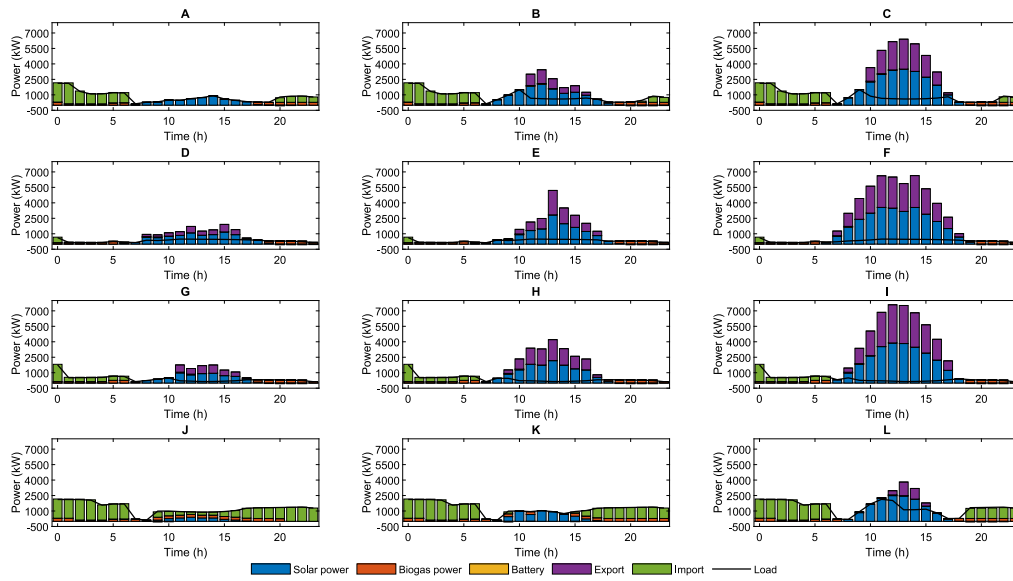


Fig. 7. Operation results of different scenarios. A B C represent typical days in spring. D E F represent typical days in summer. G H I represent typical days in autumn. J K L represent typical days in winter.

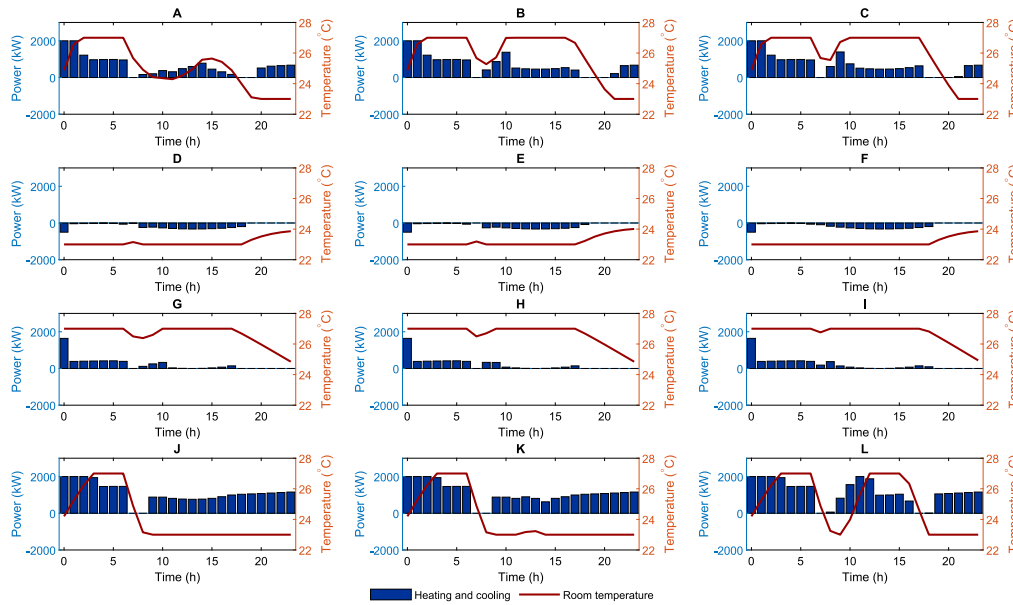


Fig. 8. Flexible heating/cooling load results in different scenarios. A B C represent typical days in spring. D E F represent typical days in summer. G H I represent typical days in autumn. J K L represent typical days in winter.

Case 3: The system planning model employing a conventional MSC operation strategy without demand-side response or battery charging/discharging strategies, but including the net-zero emissions constraint. In this case, solar PV meets demand first; excess charges batteries, then sells to the grid. If insufficient, the biogas engine supplements, then the battery discharges, and finally the grid supplies the rest.

3.3.1. Comparison between the proposed net-zero model and the non-net-zero planning model

Case 1 incorporates a net-zero emissions constraint to achieve the carbon-neutral objective. Since it might result in higher system costs, it is crucial to conduct a comparative analysis with the system planning model without the carbon constraint. Table 6 demonstrates the optimal configuration results for the rural system planning without the net-zero emissions constraint. The unconstrained model results in a significantly smaller installed PV capacity compared with the net-zero constrained

case. This reduction occurs because surplus PV generation for grid export becomes unnecessary under carbon-unconstrained conditions.

Using an emission factor of 0.5 kg CO₂ per kWh for electricity production, Table 7 illustrates that while Case 1 incurs 17% higher total annual costs than Case 2, it achieves a substantial annual reduction of 2078 tons of carbon emissions. The annualised equipment expenditure includes the initial investment, replacement, and maintenance costs of system components, converted to their annual equivalents. The annualised equipment expenditure in Case 1 is higher than that in Case 2 because Case 1 requires more PV panels to export electricity to the grid to achieve the net-zero emissions target. As shown in Figs. 9 and 10, PV panels account for 74% of the equipment expenditure in Case 1, while the biogas module makes up 74% of the total equipment cost in Case 2.

The annual net electricity purchase cost in Case 1 is negative, as the system exports more electricity to the grid than it imports to ensure

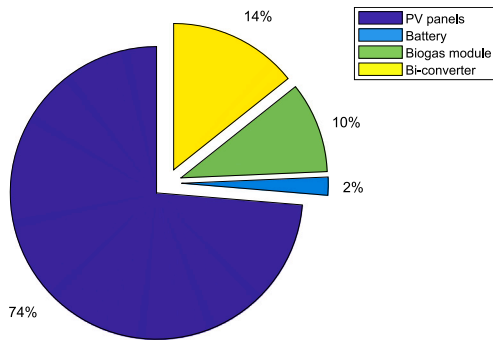


Fig. 9. Equipment expenditure breakdown by components (Case 1).

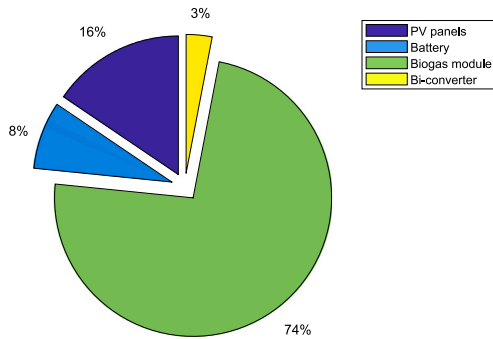


Fig. 10. Equipment expenditure breakdown by components (Case 2).

that the annual net electricity balance approaches zero. In contrast, the high annual net electricity purchase cost in Case 2 indicates a stronger dependence on grid electricity to meet load demand.

3.3.2. Comparison between the proposed strategy model and the MSC strategy model

To demonstrate the advantages of the proposed system planning model, a comparative cost analysis is conducted against the system planning model with a conventional MSC operation strategy. Fig. 11 compares the optimal planning results in Case 1 and Case 3. Case 1 features a higher PV panel capacity compared to Case 3, which consequently necessitates a greater number of bi-converters. However, the capacities of the battery storage system and the biogas engine are comparatively lower.

As shown in Table 8, Case 1 exhibits notable economic benefits, achieving a 12% reduction in total annual costs compared to Case 3. The annualised equipment expenditure in Case 1 exceeds that in Case 3, which can be attributed to the larger installed capacity of PV panels in Case 1. Despite reduced capacities of the batteries and biogas engines, the annualised equipment expenditure remains higher due to the comparatively higher unit cost of PV panels relative to batteries and biogas engines.

The annual electricity purchase cost in Case 1 is 28% lower than that in Case 3 and its annual electricity sales revenue is 3% higher. This outcome can be attributed to the operation strategy adopted in Case 1, which integrates both a demand-side response strategy and a time-of-use prices-based battery charging and discharging strategy. This operation strategy enables effective load shifting, thereby reducing electricity purchase costs. Fig. 12 illustrates the output of each component for Case 1 and Case 3 on a typical spring day. As shown, compared to Case 3, Case 1 imports more electricity from the grid between 00:00 and 07:00 due to the lower off-peak electricity price, which are used to charge the batteries and meet the maximum cooling/heating demand. In contrast, Case 3 imports a greater amount of electricity from the grid

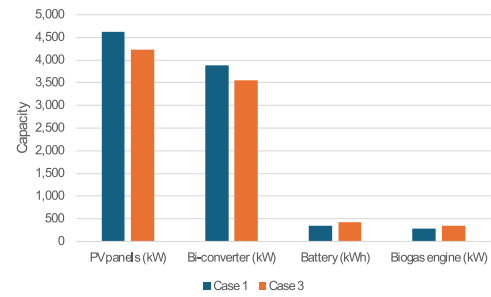


Fig. 11. Optimal planning results in Case 1 and Case 3.

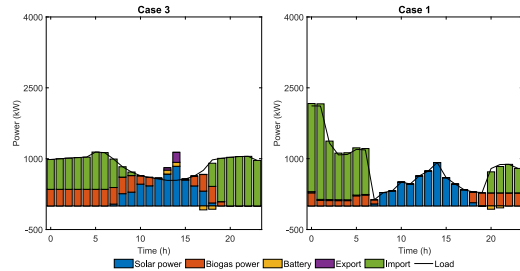


Fig. 12. Operation results of a typical day in spring (Case 1 and Case 3).

between 19:00 and 24:00. This is due to the depletion of the biogas engine and batteries during this period, forcing the system to rely on grid electricity at higher rates and thus increasing overall electricity costs.

3.4. Discussion

The results demonstrate that the proposed planning model, incorporating a novel operation strategy, achieves greater economic efficiency than the model employing a conventional MSC operation strategy. Meanwhile, the proposed zero-carbon planning model achieves significant CO₂ emission reductions with only a modest increase in total system cost compared to the non-net-zero counterpart.

As the ventilation load constitutes only a small fraction of the total energy demand of a pig farm compared to the heating and cooling loads [40], this study does not model it explicitly but instead uses surrogate data from similar pig farm loads. Future research may incorporate the influence of ventilation load on the overall load of the pig farm and develop a more detailed model for ventilation.

In this study, animal welfare in pig production was considered through a defined indoor temperature range implemented as a constraint in the model, rather than incorporating it directly into the objective function. Research that quantitatively characterises pig thermal comfort for direct integration into optimisation objectives remains limited, as most existing utility-based approaches are designed for human thermal comfort. Future studies could extend the model to incorporate pig welfare directly into the optimisation objective, allowing a more comprehensive evaluation of animal comfort and welfare.

4. Conclusion

This study proposes a net-zero stochastic planning model for pig farm-dominated rural energy systems, incorporating the agricultural demand response to optimise components sizing. The energy resources and loads associated with the pig farm are comprehensively modelled, and a novel operation strategy that accounts for agricultural demand-side flexibility is developed. Uncertainties in renewable generation and

load demand are addressed through a scenario-based stochastic optimisation framework solved using a GA. Based on comparative analyses, the main conclusions are as summarised follows:

(1) The proposed net-zero planning model successfully balances economic and environmental objectives. Despite a slight increase in total annual cost, it achieves a substantial annual reduction of 2078 tons of CO₂ emissions, demonstrating its effectiveness in balancing economic feasibility and environmental sustainability.

(2) The integration of the proposed novel operation strategy yields notable economic advantages. By strategically scheduling electricity imports during low-price periods, the strategy enables cost-effective load shifting, achieving 12% total annual cost savings compared to conventional MSC operation strategies without agricultural demand-side response.

From a practical perspective, this study offers a useful reference for designers and planners of rural energy systems. By integrating flexible agricultural loads with local natural resources and implementing the proposed operation strategy, the planning model achieves economic efficiency and significant CO₂ reductions. From a policy perspective, the proposed zero-carbon framework supports rural energy transition and decarbonisation, demonstrating that economically viable and environmentally sustainable energy systems can be developed at the village scale. It also provides valuable evidence for promoting incentive mechanisms and net-zero initiatives in rural regions. At the community level, the study presents a feasible pathway toward zero-carbon rural development, illustrating how the integration of flexible agricultural loads and local resources can enhance energy efficiency, reduce emissions, and foster sustainable and resilient rural energy infrastructure.

Building on this foundation, future research will extend the proposed framework to other agricultural sectors, particularly greenhouse cultivation, aiming to develop integrated energy systems that leverage synergies between livestock and horticultural operations.

CRedit authorship contribution statement

Shuang Kang: Writing – original draft, Software, Methodology, Conceptualization. **Wei Gan:** Writing – review & editing, Supervision. **Yue Zhou:** Writing – review & editing, Supervision, Project administration, Conceptualization. **Ping Ai:** Resources.

Declaration of competing interest

The authors declare that they have no known competing financial interests or personal relationships that could have appeared to influence the work reported in this paper.

Acknowledgments

This work is supported by the China Scholarship Council program (Project ID: 202006760091).

Data availability

Data will be made available on request.

References

- Puig D, Farrell TC, Moner-Girona M. A quantum leap in energy efficiency to put the sustainable development goals in closer reach. *Glob Policy* 2018;9(3):429–31. <http://dx.doi.org/10.1111/1758-5899.12574>.
- Khirennas A, Talha A, Kaabeche A, Bakelli Y. Overview of fossil fuel-based hybrid power generation systems within mini-grids—the experience of storage-less PV system integration into three of the great Algerian south mini-grids. *Energy Convers Manage* 2020;221:113191. <http://dx.doi.org/10.1016/j.enconman.2020.113191>.
- Thomas A, Racherla P. Constructing statutory energy goal compliant wind and solar PV infrastructure pathways. *Renew Energy* 2020;161:1–19. <http://dx.doi.org/10.1016/j.renene.2020.06.141>.
- Long H, Fu X, Kong W, Chen H, Zhou Y, Yang F. Key technologies and applications of rural energy internet in China. *Inf Process Agric* 2024;11(3):277–98. <http://dx.doi.org/10.1016/j.inpa.2022.03.001>.
- Fu X, Zhou Y. Collaborative optimization of PV greenhouses and clean energy systems in rural areas. *IEEE Trans Sustain Energy* 2023;14(1):642–56. <http://dx.doi.org/10.1109/TSTE.2022.3223684>.
- Kumar P, Pal N, Sharma H. Optimization and techno-economic analysis of a solar photo-voltaic/biomass/diesel/battery hybrid off-grid power generation system for rural remote electrification in eastern India. *Energy* 2022;247:123560. <http://dx.doi.org/10.1016/j.energy.2022.123560>.
- Zhi Y, Yang X. Scenario-based multi-objective optimization strategy for rural PV-battery systems. *Appl Energy* 2023;345:121314. <http://dx.doi.org/10.1016/j.apenergy.2023.121314>.
- Yang Z, Sun G, Behrens P, Østergaard PA, Egusquiza E, Xu B, Chen D, Patelli E. The potential for photovoltaic-powered pumped-hydro systems to reduce emissions, costs, and energy insecurity in rural China. *Energy Convers Manage X* 2021;11:100108. <http://dx.doi.org/10.1016/j.ecmx.2021.100108>.
- Fu X, Zhou Y, Wei Z, Wang Y. Optimal operation strategy for a rural microgrid considering greenhouse load control. *CSEE J Power Energy Syst* 2023;1–11. <http://dx.doi.org/10.17775/CSEEJPES.2022.06200>.
- Li W, Zou Y, Yang H, Fu X, Xiang S, Li Z. Two stage stochastic energy scheduling for multi energy rural microgrids with irrigation systems and biomass fermentation. *IEEE Trans Smart Grid* 2024;1. <http://dx.doi.org/10.1109/TSG.2024.3483444>.
- Liu Y, Xu X, Xu L, Liu Y, Liu J, Hu W, Yang N, Jawad S, Luo Y. Multi-timescale collaborative operation of renewable energy-based power system and Agri-product supply chain considering dynamic energy consumption-based crop growth. *Appl Energy* 2025;377:124359. <http://dx.doi.org/10.1016/j.apenergy.2024.124359>.
- Kwak Y, Shin H, Kang M, Mun S-H, Jo S-K, Kim S-H, Huh J-H. Energy modeling of pig houses: A South Korean feasibility study. *Energy Strat Rev* 2021;36:100672. <http://dx.doi.org/10.1016/j.esr.2021.100672>.
- Shin H, Kwak Y, Jo S-K, Kim S-H, Huh J-H. Calibration of building energy simulation model for a mechanically ventilated livestock facility. *Biosyst Eng* 2022;217:115–30. <http://dx.doi.org/10.1016/j.biosystemeng.2022.03.009>.
- Hatzigiorgiou N. *Microgrids: Architectures and control*. Wiley-IEEE Press; 2014. <http://dx.doi.org/10.1002/9781118720684>.
- Lü X, He S, Xu Y, Zhai X, Qian S, Wu T, WangPei Y. Overview of improved dynamic programming algorithm for optimizing energy distribution of hybrid electric vehicles. *Electr Power Syst Res* 2024;232:110372. <http://dx.doi.org/10.1016/j.epsr.2024.110372>.
- Zhu D, Pritchard E, Dadam SR, Kumar V, Xu Y. Optimization of rule-based energy management strategies for hybrid vehicles using dynamic programming. *Combust Engines* 2021;184(1):3–10. <http://dx.doi.org/10.19206/ce-131967>.
- Bukar AL, Tan CW, Yiew LK, Ayop R, Tan W-S. A rule-based energy management scheme for long-term optimal capacity planning of grid-independent micro-grid optimized by multi-objective grasshopper optimization algorithm. *Energy Convers Manage* 2020;221:113161. <http://dx.doi.org/10.1016/j.enconman.2020.113161>.
- Gallagher K, Sambridge M. Genetic algorithms: A powerful tool for large-scale nonlinear optimization problems. *Comput Geosci* 1994;20(7):1229–36. [http://dx.doi.org/10.1016/0098-3004\(94\)90072-8](http://dx.doi.org/10.1016/0098-3004(94)90072-8).
- Ghanbari K, Maleki A, Rezaei Ochbelagh D. Optimal design of solar/wind/energy storage system-powered ro desalination unit: Single and multi-objective optimization. *Energy Convers Manage* 2024;315:118768. <http://dx.doi.org/10.1016/j.enconman.2024.118768>.
- Munoz-Pincheira JL, Salazar L, Sanhueza F, Lüer-Villagra A. Optimizing the design of stand-alone hybrid renewable energy systems with storage using genetic algorithms: Analysis of the impact of temporal complementarity of wind and solar sources. *Energy Convers Manage* 2025;341:120016. <http://dx.doi.org/10.1016/j.enconman.2025.120016>.
- Zhang Y, Ma T, Elia Campana P, Yamaguchi Y, Dai Y. A techno-economic sizing method for grid-connected household photovoltaic battery systems. *Appl Energy* 2020;269:115106. <http://dx.doi.org/10.1016/j.apenergy.2020.115106>.
- Hassan R, Das BK, Hasan M. Integrated off-grid hybrid renewable energy system optimization based on economic, environmental, and social indicators for sustainable development. *Energy* 2022;250:123823. <http://dx.doi.org/10.1016/j.energy.2022.123823>.
- Bacha B, Ghodbane H, Dahmani H, Betka A, Toumi A, Chouder A. Optimal sizing of a hybrid microgrid system using solar, wind, diesel, and battery energy storage to alleviate energy poverty in a rural area of Biskra, Algeria. *J Energy Storage* 2024;84:110651. <http://dx.doi.org/10.1016/j.est.2024.110651>.
- Jaman A, Das BK, Mahim M, Hasan A, Siddika S, Ahmed MM, Okonkwo PC. Techno-econo-environmental analysis of sustainable hybrid solar-wind-biogas using municipal solid waste-based grid independent power plant with dual mode energy storage strategy. *Energy* 2024;307:132777. <http://dx.doi.org/10.1016/j.energy.2024.132777>.
- Kallel R, Boukettaya G. An energy cooperative system concept of DC grid distribution and PV system for supplying multiple regional AC smart grid connected houses. *J Build Eng* 2022;56:104737. <http://dx.doi.org/10.1016/j.job.2022.104737>.

- [26] Zou B, Peng J, Li S, Li Y, Yan J, Yang H. Comparative study of the dynamic programming-based and rule-based operation strategies for grid-connected PV-battery systems of office buildings. *Appl Energy* 2022;305:117875. <http://dx.doi.org/10.1016/j.apenergy.2021.117875>.
- [27] Liu J, Wang M, Peng J, Chen X, Cao S, Yang H. Techno-economic design optimization of hybrid renewable energy applications for high-rise residential buildings. *Energy Convers Manage* 2020;213:112868. <http://dx.doi.org/10.1016/j.enconman.2020.112868>.
- [28] Liu J, Chen X, Yang H, Li Y. Energy storage and management system design optimization for a photovoltaic integrated low-energy building. *Energy* 2020;190:116424. <http://dx.doi.org/10.1016/j.energy.2019.116424>.
- [29] Alimohammadisagvand B, Jokisalo J, Sirén K. Comparison of four rule-based demand response control algorithms in an electrically and heat pump-heated residential building. *Appl Energy* 2018;209:167–79. <http://dx.doi.org/10.1016/j.apenergy.2017.10.088>.
- [30] Sun L, Li J, Chen L, Xi J, Li B. Energy storage capacity configuration of building integrated photovoltaic-phase change material system considering demand response. *IET Energy Syst Integr* 2021;3(3):263–72. <http://dx.doi.org/10.1049/esi2.12013>.
- [31] Reay DS, Davidson EA, Smith KA, Smith P, Melillo JM, Dentener F, Crutzen PJ. Global agriculture and nitrous oxide emissions. *Nat Clim Chang* 2012;2(6):410–6. <http://dx.doi.org/10.1038/nclimate1458>.
- [32] Wu C. Carbon emission evaluation and low carbon economy optimization scheduling of rural integrated energy system based on LCA method. *IEEE Access* 2025;13:17182–94. <http://dx.doi.org/10.1109/ACCESS.2025.3533099>.
- [33] Jiang F, Xiao C, Yi Z, He G, Guo Q, Peng X, Xiao G. Multi-energy cooperation and low-carbon operation strategy of eco-agricultural integrated energy system containing photovoltaic and biomass energy. *Proc CSEE* 2024;44(4):1221–39. <http://dx.doi.org/10.13334/j.0258-8013.pcsee.222606>.
- [34] Araoye TO, Ashigwuike EC, Mbunwe MJ, Bakinson OI, Ozue TI. Techno-economic modeling and optimal sizing of autonomous hybrid microgrid renewable energy system for rural electrification sustainability using HOMER and grasshopper optimization algorithm. *Renew Energy* 2024;229:120712. <http://dx.doi.org/10.1016/j.renene.2024.120712>.
- [35] Pal A, Bhattacharjee S. Effectuation of biogas based hybrid energy system for cost-effective decentralized application in small rural community. *Energy* 2020;203:117819. <http://dx.doi.org/10.1016/j.energy.2020.117819>.
- [36] Wang Q, Xiao Y, Tan H, Mohamed MA. Day-ahead scheduling of rural integrated energy systems based on distributionally robust optimization theory. *Appl Therm Eng* 2024;246:123001. <http://dx.doi.org/10.1016/j.applthermaleng.2024.123001>.
- [37] Rahimian H, Mehrotra S. Frameworks and results in distributionally robust optimization. *Open J Math Optim* 2022;3:1–85. <http://dx.doi.org/10.5802/ojmo.15>.
- [38] Islam MM, Mun H-S, Bostami ABMR, Ahmed ST, Park K-J, Yang C-J. Evaluation of a ground source geothermal heat pump to save energy and reduce CO₂ and noxious gas emissions in a pig house. *Energy Build* 2016;111:446–54. <http://dx.doi.org/10.1016/j.enbuild.2015.11.057>.
- [39] Alberti L, Antelmi M, Angelotti A, Formentin G. Geothermal heat pumps for sustainable farm climatization and field irrigation. *Agricult Water Manag* 2018;195:187–200. <http://dx.doi.org/10.1016/j.agwat.2017.10.009>.
- [40] Christian S, Dirk W, Stephan F. Energy for heating and ventilation in pig production on farms. *Landtechnik* 2009;64(6):423–5, URL: <https://www.agricultural-engineering.eu/landtechnik/article/download/2009-64-6-423-425/2009-64-6-423-425-en-pdf/1099>.
- [41] Yin R, Lu H, Gong C. Optimization calculation method for biogas production from different types of livestock and poultry manure. *China Biogas* 2023;41(3):91–6. <http://dx.doi.org/10.20022/j.cnki.1000-1166.2023030091>.
- [42] Verbeke S, Audenaert A. Thermal inertia in buildings: A review of impacts across climate and building use. *Renew Sustain Energy Rev* 2018;82:2300–18. <http://dx.doi.org/10.1016/j.rser.2017.08.083>.
- [43] Prairie Swine Centre. Energy efficiency in barns: Part I. 2014, URL: [https://prairieswine.com/rsc/publications-psc/pdf-fact/Energy Efficiency Part 1.pdf](https://prairieswine.com/rsc/publications-psc/pdf-fact/Energy%20Efficiency%20Part%201.pdf).
- [44] Scaillierez A, Boumans I, van Nieuwamerongen S, van der Tol P, Bokkers E. Can artificial light enlighten pig welfare? In: Proceedings of the 8th international conference on the assessment of animal welfare at farm and group level. Netherlands: Wageningen Academic Publishers; 2021, p. 114, 8th International Conference on The Assessment of Animal Welfare at Farm and Group Level, WAFL 2021 ; Conference date: 16-08-2021 Through 19-08-2021.
- [45] Duffie JA, Beckman WA. Available solar radiation. In: *Solar engineering of thermal processes*. John Wiley & Sons, Ltd; 2013, p. 43–137. <http://dx.doi.org/10.1002/9781118671603.ch2>.
- [46] Wen L, Jiang W. Bi-level capacity optimization of electricity-hydrogen coupled energy system considering power curtailment constraint and technological advancement. *Energy* 2024;307:132603. <http://dx.doi.org/10.1016/j.energy.2024.132603>.
- [47] Lin S, Liu C, Shen Y, Li F, Li D, Fu Y. Stochastic planning of integrated energy system via frank-copula function and scenario reduction. *IEEE Trans Smart Grid* 2022;13(1):202–12. <http://dx.doi.org/10.1109/TSG.2021.3119939>.
- [48] Xiang Y, Cai H, Gu C, Shen X. Cost-benefit analysis of integrated energy system planning considering demand response. *Energy* 2020;192:116632. <http://dx.doi.org/10.1016/j.energy.2019.116632>.
- [49] Sengupta M, Xie Y, Lopez A, Habte A, Maclaurin G, Shelby J. The national solar radiation data base (NSRDB). *Renew Sustain Energy Rev* 2018;89:51–60. <http://dx.doi.org/10.1016/j.rser.2018.03.003>.
- [50] Yuan P, Duanmu L, Wang Z, Gao K, Zhao X, Liu X, Kong W. Electricity consumption and load prediction method for Chinese rural residences based on the randomness and seasonality in electricity usage behavior. *Energy Build* 2023;279:112647. <http://dx.doi.org/10.1016/j.enbuild.2022.112647>.